Chapter 1

Introduction

1.1 Particle physics and future colliders

Particle physics is on the verge of extending knowledge to the terascale, energies of tera-electronvolts. The Large Hadron Collider (LHC) will collide protons up to a centre of mass energy of 14 TeV and make discoveries. Predicted particles such as the Higgs, weakly interacting massive particles (WIMPs) and supersymmetric (SUSY) particles may be found. But it is up to the International Linear Collider (ILC) to measure the properties of the LHC discoveries, the precision masses and the couplings, without assuming models in the process, to determine whether the particles discovered are parts of larger families, to differentiate between the theories and to delve into CP-violation. Both machines working together should be able to shed light on undiscovered principles of nature, dark matter, extra dimensions, unification at energies around 10^{15} GeV, the families of particles, the origin of the universe and the dominance of matter over anti-matter.

1.1.1 The Standard Model

The current theory of fundamental particles and their interactions, known as the Standard Model (SM) [1], has been hugely successful. The SM contains (table 1.1) twelve fermions and four vector bosons mediating three elementary forces: strong, weak and electromagnetic. Seven of these particles (the charm quarks, bottom quarks, top quarks, tau neutrinos, gluons and the W and Z bosons) were predicted by the SM before they were discovered. There is also the scalar boson known as the Higgs that gives the fermions mass within the SM and breaks the electroweak symmetry. This Higgs boson is yet to be discovered.

There is a force not included in the SM: gravity. Plus, there are at least 19 parameters that need to be measured and put in by hand, not fundamentally derived. Despite its success to date, the SM is an incomplete description of the particles and forces in the universe.

Fermions					
Leptons			Quarks		
ν_e	ν_μ	ν_τ	u	s	t
e	μ	τ	d	c	b

Force	Mediating Boson
Weak	$W^{\pm}$, Z^0
Electromagnetic	γ
Strong	gluons
Higgs	H^0

Table 1.1: The Standard Model [2].

1.1.2 Why look towards the Terascale?

Particle physics knowledge, as summarised in the SM, is missing some vital parts. There is much more to be discovered and there are various hints that the place to look next is in the region from 100 GeV to the TeV scale.

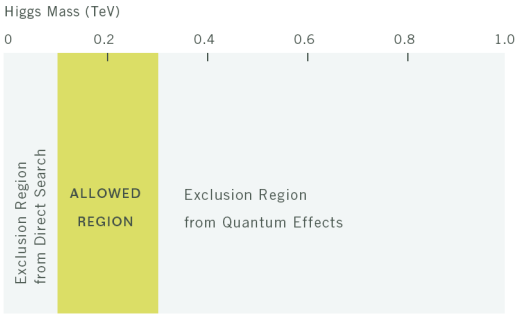
Higgs Boson

The Higgs mechanism [3] specifies a potential for the vacuum state leading to spontaneous symmetry breaking of the electroweak force. The Higgs boson and the W and Z bosons acquire masses. The Higgs mass, however, is not predicted and until it is found, the Standard Model is not complete.

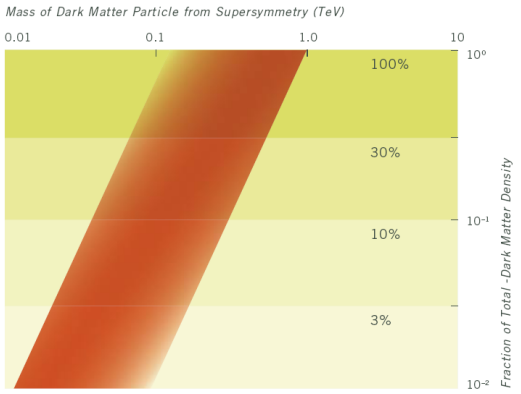
The Higgs mechanism introduces longitudinal polarisation to the bosons which mediate electroweak processes at high energy. This breaks unitarity *unless* the Higgs is light and couples to the fermions and bosons as predicted in the SM, thereby cancelling processes and leading to finite cross-sections [4]. In order to satisfy unitarity in the scattering of longitudinal W and Z bosons ($2W_L^+W_L^- + Z_LZ_L$), the Higgs mass must be < 780 GeV [5]. Otherwise, the Standard Model fails around 1 TeV. New physics around 1 TeV could also solve this unitarity problem but there is no theory that generates the necessary cancellations as naturally as the "light" Higgs. Therefore, SM theory requires a Higgs under 1 TeV or, failing that, there **must** be new physics around 1 TeV.

However, the Higgs in the SM is allowed to have an infinite mass in the absence of fine tuning [4]. The "Hierarchy Problem" creates an infinite Higgs mass via fermion loops, where the fermions can have any momenta and give infinite and diverging mass corrections. It becomes necessary to impose an energy cut-off after which the SM fails and new physics exists. Using the Planck mass as the point where the SM fails produces a Higgs mass nearly as high as the Planck mass, much larger than the light Higgs required to satisfy unitarity. Therefore there must be new physics to stabilise the light Higgs mass and it is expected around 1 TeV.

Experimental searches for the SM Higgs have narrowed the range of its mass as depicted in figure 1.1(a). Direct searches at the Large Electron-Positron Collider (LEP) showed a lower limit (95% confidence level) of 114 GeV [6]. Precise measurements of electroweak observables with recent measurements of the top mass and W boson mass at the Tevatron [7] have suggested an upper limit of 144 GeV (also at the 95% confidence level).



(a) The mass range of the SM Higgs is shown as the coloured region bounded by direct Higgs searches at the lower limit and precision measurements of electroweak observables at the higher limit. Recent data has narrowed the window further to 114 - 144 GeV [7].



(b) The mass of SUSY dark matter candidates versus the amount of observed dark matter in the universe that they can account for. The shaded region roughly indicates the theoretically allowed values for the amount of each SUSY mass left over from the Big Bang as a fraction of the experimentally observed dark matter.

Figure 1.1: The terascale is predicted to contain the Higgs and dark matter candidates [8].

Supersymmetry

The hierarchy problem can be solved with Supersymmetry [4] (SUSY) which, in the minimal supersymmetric model, introduces two scalars for every fermion with matching couplings to cancel the diverging mass terms. Five physical Higgs are predicted: H^+, H^-, A°, h° and H° (other supersymmetry theories can predict more). In general SUSY theories, the lightest Higgs (h°) is predicted to be under 200 GeV and other supersymmetric partners are predicted to be under 1 TeV [6].

If this is the new physics required to stabilise the Higgs mass, the terascale is the place to look.

Dark Matter

Astrophysical observations indicate that not only is dark (non-luminous and non-absorbing) matter present in the universe but it is more than five times more common than baryonic matter [9]. By measuring the density of the dark matter particles (the thermal relic density) and invoking theories independent of particle physics, astrophysics studies suggest that dark matter masses lie under 1 TeV [10]. Dark matter candidates that arise from particle physics theories include weakly interacting massive particles with masses between 10 GeV and 1 TeV. The most likely candidate is the lightest supersymmetric particle with proposed mass below 1 TeV [6]. As shown in figure 1.1(b), SUSY particles with terascale masses could account for the vast proportion of observed dark matter. Other dark matter candidates include Kaluza-Klein particles (also with a predicted mass below 1 TeV) [8].

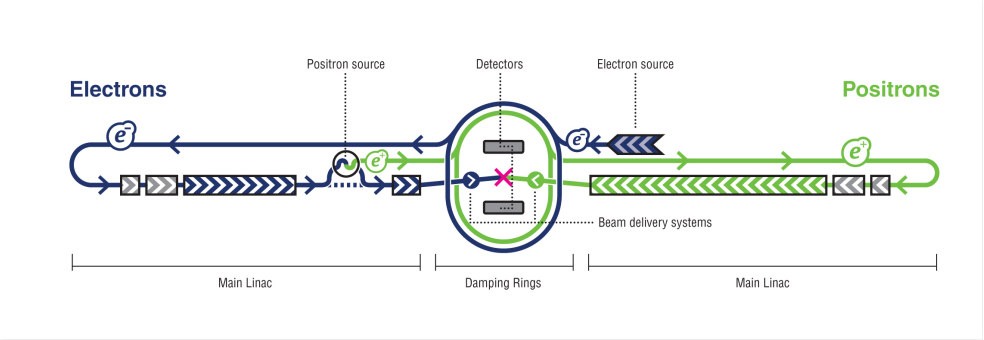


Figure 1.2: A schematic of the ILC layout [13].

The convergence of astrophysics and particle physics predictions points to the terascale as an extremely promising area to search for dark matter.

Grand Unified Theories

Precise measurements of the SM couplings demonstrated that the strong, electromagnetic and weak forces did not unify at one point at very high energies [6]. The coupling constants do meet, however, in many Grand Unified Theories (GUTs) such as supersymmetry and other models that introduce new physics around 1 TeV.

The discovery of terascale physics could lead neatly to unification of forces at higher energy scales or hold new surprises.

1.1.3 What is the ILC?

The International Linear Collider (ILC) is a proposed high energy electron-positron collider with centre of mass energies $\sqrt{s}$ from 200 to 500 GeV or 1 TeV with the proposed future upgrade. The $\sqrt{s}$ and polarisation of the electron beam (if required) will be controllable at the 0.1% level [11].

The ILC uses 11 km linear accelerators (linacs) to accelerate the electrons and positrons. It was decided to use superconducting radio frequency (RF) accelerating cavities following the recommendation of the International Technology Recommendation Panel in 2004 [12].

Figure 1.2 shows a schematic of the ILC. A photocathode DC gun is used as the electron source (with greater than 80% polarisation) and the positrons are produced from an undulator. The electrons and positrons enter damping rings of 6.7 km circumference. There is beam transport to the linac which comprises of 31.5 MV/m superconducting cavities. There is 4.5 km of beam delivery system bringing the two beams to the interaction point (IP).

The ILC has been designed to deliver 500 fb^{-1} of integrated luminosity within four years. Its pulse rate is 5 Hz and each pulse is $\sim$1 ms long, comprising 1000-6000 bunches each of $(1-2)\times10^{10}$ electrons or positrons. A plane of accelerator parameters has been defined over which the ILC can operate. These accelerator parameter schemes are shown in tables 1.2

Parameter	1.TESLA	2.USSC
N	2×10^{10}	2×10^{10}
N bunches	2820	2820
Bunch spacing (ns)	336.9	336.9
IP σ_x (nm)	554	543
IP σ_y (nm)	5.0	5.7
IP σ_z (μm)	300	300
Luminosity ($m^{-2}s^{-1}$)	2.94×10^{38}	2.57×10^{38}

Parameter	3.Nominal	4.Low Q	5.Large Y	6.Low P	7.High Lum
N particles	2×10^{10}	1×10^{10}	2×10^{10}	2×10^{10}	2×10^{10}
N bunches	2820	5640	2820	1330	2820
Bunch spacing (ns)	307.7	153.8	307.7	461.5	307.7
IP σ_x (nm)	655	495	495	452	452
IP σ_y (nm)	5.7	3.5	8.1	3.8	3.5
IP σ_z (μm)	300	150	500	200	150
Luminosity ($m^{-2}s^{-1}$)	2.03×10^{38}	2.01×10^{38}	2.00×10^{38}	2.05×10^{38}	4.92×10^{38}

Table 1.2: Shown are a few parameters of interest for the seven schemes proposed for the 500 GeV operation of the ILC with 31.5 MV/m gradient [14]. Two schemes are historical parameter sets described in preliminary documentation (the TESLA Technical Design Report [15], TESLA, and the US Technology Options Study [16], USSC). The remaining five schemes describe a "plane" that allows for flexibility when the accelerator is in operation. For each parameter in this plane, the lowest value has been highlighted (dark grey) and the highest value has been highlighted (light grey).

(for the 500 GeV centre of mass ILC) and 1.3 (for the proposed 1 TeV upgrade).

1.1.4 Why a linear collider?

The electron-positron collider has to be a linear accelerator and not a circular one at these energies. In a circular accelerator, such as the LHC, the collision particles are accelerated in a circle losing energy through synchrotron radiation due to the transverse acceleration[1] at a rate proportional to γ^4 (where γ is the Lorentz factor E/m_0c^2) as shown in equation 1.1 [17]. P_γ is the power lost to the synchrotron radiation, e is the particle charge, β is the particle velocity as a fraction of the speed of light and ρ is the bending radius. Since the rate is inversely proportional to the mass to the power of four and directly proportional to the energy to the power of four, it poses a limit on the energy of light particles such as electrons and positrons that can be accelerated in a circular accelerator. Low mass and high energy particles such as 250 GeV electrons or positrons will lose a lot of energy through synchrotron radiation, which is deposited into the vacuum components of the collider and needs to be replaced in the beam by the accelerating cavities. For the LEP ring (with circumference 27 km [18]), a 250 GeV electron (or positron) beam loses 80 GeV through synchrotron

[1]Energy is also lost due to acceleration parallel to the direction of the particle (as in a linear accelerator) but it only depends on the acceleration force. For the same acceleration force, transverse acceleration leads to more power in synchrotron radiation by a factor of γ^2, which is very large for these relativistic machines. The loss of energy due to synchrotron radiation from parallel acceleration is not significant [17].

Parameter	8.TESLA	9.USSC
N particles	1.4×10^{10}	2×10^{10}
N bunches	4886	2820
Bunch spacing (ns)	175.4	336.9
IP σ_x (nm)	392	489
IP σ_y (nm)	2.8	4.0
IP σ_z (μm)	300	300
Luminosity ($m^{-2}s^{-1}$)	5.07×10^{38}	3.81×10^{38}

Parameter	10.Nominal	11.Low Q	12.Large Y	13.Low P	14.High Lum
N particles	2×10^{10}	1×10^{10}	2×10^{10}	2×10^{10}	2×10^{10}
N bunches	2820	5640	2820	1330	2820
Bunch spacing (ns)	307.7	153.8	307.7	461.5	307.7
IP σ_x (nm)	554	392	367	350	320
IP σ_y (nm)	3.5	2.5	7.0	2.7	2.5
IP σ_z (μm)	300	150	600	200	150
Luminosity ($m^{-2}s^{-1}$)	2.82×10^{38}	2.84×10^{38}	2.92×10^{38}	2.92×10^{38}	7.88×10^{38}

Table 1.3: Shown are a few parameters of interest for the seven schemes proposed for the energy upgraded operation of the ILC with 31.5 MV/m gradient [14]. Two schemes are historical parameter sets described in preliminary documentation (the TESLA Technical Design Report [15], TESLA, and the US Technology Options Study [16], USSC). The TESLA scheme is for 800 GeV and all other schemes are for 1 TeV centre of mass energy. The remaining five schemes describe a "plane" that allows for flexibility when the accelerator is in operation. For each parameter in this plane, the lowest value has been highlighted (dark grey) and the highest value has been highlighted (light grey).

radiation per turn and a 365 GeV beam would need to have its full beam energy replaced by accelerating cavities in every turn. However, the amount of power deposited in the collider components creates the strictest limit to how much synchrotron radiation can be tolerated. LEP was running at the limit of the hardware constituents with 100 GeV beam energy by depositing 18 MW through synchrotron radiation [18]. With 250 GeV beams forty times this power would be dumped.

$$P_\gamma = \frac{2}{3} e^2 \frac{c\beta^4\gamma^4}{\rho^2} \tag{1.1}$$

1.1.5 Why an electron-positron collider?

The LHC at CERN is a discovery machine capable of finding the evidence for the Higgs, dark matter candidates, extra dimensions, supersymmetric particles and other new physics. However, proton on proton colliders do not have great sensitivity. The nominal centre of mass energy of the collider is 14 TeV but the actual interactions involve the particles within the proton, the quarks and gluons, whose momenta are not precisely known in each event. Although the mass of the Higgs can be measured to 0.1% [19] and the couplings to gauge bosons and fermions measured to 10-40% [20], the Higgs self-coupling cannot be measured and theoretical assumptions have to be made. It would also be difficult to tell a SM Higgs from a Higgs from another model such as the h^0 of MSSM.

Electron-positron colliders are measuring machines with greater sensitivity. The collisions are of a known energy and polarisation. There are also lower event rates, less background and lower radiation doses, allowing precision measurements, tracking and particle identification. It is required to take the LHC discoveries a step further, to complement the LHC and to understand the physics behind the discoveries.

The ILC measures properties to greater accuracy plus properties that the LHC cannot measure such as the Higgs trilinear self-coupling, Higgs decay branching ratios and total decay width and absolute values of coupling constants without assuming models [11]. Subtle effects in the measurements below 1 TeV could hold clues for physics at even higher energies and these would be apparent with the precision ILC measurements. For example, some models that include extra dimension predict a particle called the radion which mixes with the Higgs and reduces the strength of the interaction between the Higgs and SM particles [11]. Therefore, precision ILC measurements of the interactions can indicate the presence of extra dimensions.

The ILC is better equipped than the LHC to answer the cosmological questions of how many dimensions there are. The LHC is able to detect Kaluza-Klein gravitons, which are one signature that indicates extra dimensions, but it cannot extract information about them since the fundamental particles involved in the collision could have energies above the scale where this new physics comes into play. The ILC, however, with its e^+e^- collision of known energy, can measure the number of extra dimensions and their shape and size [21].

Likewise, the ILC can answer the question of the observed dark matter in the universe.

The LHC can only find dark matter candidates and derive information from the discoveries assuming theoretical models; the ILC would be needed to provide the model-independent measurements that reveal how much the dark matter candidates contribute to the dark matter in the universe and so whether they account fully for the astrophysics observations of dark matter [21].

SUSY decays are complicated and their cascade decay products hide the properties of the supersymmetric particles. The ILC can focus on one supersymmetric partner at a time by tuning the beam energy to scan the energies where they are produced [8]. It can then make precision measurements of the superparticle's mass, spin and couplings to confirm that it is the partner to a SM particle and also gather information on how the symmetry is broken. The LHC lacks the resolving power to measure superparticle interactions to the level of precision required to test the symmetry of the SUSY theory, due to the complicated decays and high SUSY backgrounds [21].

Greater sources of CP violation need to be found to explain why there is more matter than anti-matter in the universe, such as a family of Higgs or Higgs-like particles or SUSY. It will be hard to extract CP properties from particle decays and interactions in the Higgs sector or with SUSY sectors without precisely knowing the initial conditions. The ILC could be the only collider able to extract information about CP violation this way [8].

The ILC is more than just the second act though; running alongside the LHC it can feed back analyses to improve the LHC's identification and measurement of particles (or sparticles) and their properties [22].

1.2 Backgrounds at the ILC Interaction Point

Backgrounds are unavoidable. These unwanted particles and signals in detectors come from sources including off-orbit particles in the beam tails interacting near the IP, muons from beam tail collimation and synchrotron radiation photons; but the greatest contribution to IP backgrounds comes from the beam-beam interaction producing beamstrahlung and e^+e^- pairs. These are mainly forward and background going particles with little transverse momentum. This results in a "dead cone" in the very forward region of a detector where instrumentation is difficult.

1.2.1 Principal sources of IP backgrounds

Close to the IP the most important backgrounds are from the beam-beam interaction, which includes the processes beamstrahlung, pair generation, hadron production and bremsstrahlung.

Beamstrahlung

During an e^+e^- collision, each bunch is deformed under the high electromagnetic field of the other, radiating photons in a process termed beamstrahlung. Beamstrahlung is a stochas-

tic process where the probability that a particle radiates a photon of a certain energy is dependent on the field density of an oncoming beam of charged particles. The amount of beamstrahlung increases with more charged particles in the oncoming bunch and the bunch dimensions (equation 1.2) where B is the magnetic field strength of the oncoming (Gaussian) bunch, N_b the number of electrons (or positrons) in it and $\sigma_{x,y,z}$, its dimensions [23].

$$B \simeq \frac{1}{4\pi\varepsilon_0 c}\frac{5eN_b}{6\sigma_z(\sigma_x+\sigma_y)} \tag{1.2}$$

Beamstrahlung results in a beam energy spread which would be carried down to analysis as a lack of precision in measurement of masses. To suppress beamstrahlung without changing the luminosity ($\sim \frac{1}{\sigma_x\sigma_y}$), flat beams are used so that $\sigma_y << \sigma_x$.

The majority of beamstrahlung photons form a narrow cone that follows the beam straight down the extraction line, away from the IP [11].

Pair Generation

The beamstrahlung photons can exchange energy-momentum with electromagnetic fields producing e^+e^- pairs. This is called coherent pair production. Calculations show that this is in fact negligible for centre of mass energies under 1 TeV.

Incoherent pair production processes dominate in beam-beam interactions at ILC energies. Approximately 10^5 e^+e^- pairs [24] are produced through individual scattering events such as two real beamstrahlung photons (the Breit-Wheeler process, equation 1.3), one real photon and one virtual photon (the Bethe-Heitler process, equation 1.4) and two virtual photons (the Landau-Lifshitz process, equation 1.5) [23].

$$\gamma\gamma \rightarrow e^+e^- \tag{1.3}$$

$$e^\pm\gamma \rightarrow e^\pm e^+e^- \tag{1.4}$$

$$e^+e^- \rightarrow e^+e^-e^+e^- \tag{1.5}$$

Simulations of the beam-beam interaction at the ILC have shown the Bethe-Heitler process to account for over 70% of the pairs [25].

After production, the pairs experience the electromagnetic fields of the oncoming bunch. The particle that is the same charge as the oncoming bunch oscillates in its field. The particle that is the opposite charge as the oncoming bunch is deflected and so has slightly higher transverse momentum [26].

Hadron and Minijet Production

Beamstrahlung photons interact to produce hadrons or jets that are of low energies ("minijets") compared to jets from the e^+e^- interaction at the IP [24]. The hadrons are mostly produced with small transverse momentum and low energies and they continue along the

beam direction. Minijets have large transverse momentum. Both are produced at low rates: one hadronic event only occurs every few bunch crossings in simulations with TESLA parameters [24].

Bremsstrahlung

Bremsstrahlung, literally braking radiation, occurs when an individual particle scatters off the field of another particle and emits a photon. In the beam-beam interaction, electrons and positrons can scatter with either the initial or final states emitting a photon and hence losing energy through bremsstrahlung ($e^+e^- \rightarrow e^+e^-\gamma$). This results in a spent beam with particles in a low energy tail [24] plus bremsstrahlung photons.

This process are sometimes be referred to as Compton scattering of an electron with a virtual photon [24] or radiative Bhabha scattering [27]. The electrons and positrons that have lost energy through bremsstrahlung are referred to as bremsstrahlung leptons in this thesis.

1.3 The Beam-Beam Effect on Luminosity

The beam-beam interaction causes backgrounds and also affects the luminosity.

The field of the oncoming beam is transverse due to Lorentz contraction of the associated EM fields. The longitudinal coordinates of the two beams therefore need to be essentially the same for the charged particles in one beam to experience the electromagnetic field of the another. The beam-beam effect therefore occurs at the IP and depends greatly on the field created by the colliding bunches which, as in equation 1.2, depends on the dimensions of the beam and number of charged particles in it.

A useful parameter to describe the beam-beam interaction is the disruption factor $D_{x(y)}$ defined in equation 1.6, where r_e is the classical electron radius and the other variables as defined before [28]. For the ILC Nominal 500 GeV accelerator parameter set, D_x is 0.16 and D_y 18.5 [14].

$$D_{x(y)} \equiv \frac{2N_b r_e}{\gamma} \frac{\sigma_z}{\sigma_{x(y)}(\sigma_x + \sigma_y)} \tag{1.6}$$

If $D << 1$ (as is the case with D_x) and the beams are oppositely charged, the beam acts like a thin lens, focusing the beam, due to the mutual attraction of opposite charges. This is the "pinch effect" and it enhances the luminosity by about a factor of two.

If $1 < D \leq 10$, the force between the attracted beams is large enough that the kick it produces brings the beam centres closer and small offsets in their incoming trajectories do not result in a significant loss in luminosity.

However, at the ILC, $D_y = 18.5$ and the beam-beam effects lead to an instability known as the kink instability. Internal beam distortions are resonantly amplified and the beams

oscillate in the vertical plane. This leads to a situation where even a small offset in position or angle at the IP results in a large luminosity loss [29].

The outgoing angle of the full energy particles (Θ_y) after this beam-beam kick is related to the initial offset of the two beams in position (Δ_y) as shown in equation 1.7 [30].

$$\Theta_y = \frac{1}{2} D_y F \frac{\Delta_y}{\sigma_z} \tag{1.7}$$

For small position offsets, F is a constant and the relationship between position offset and angle kick is linear. F is empirically found through simulations to depend on the disruption factor such that the larger D_y, the larger the region where the kick is proportional to the position offset. This is a useful way of measuring the position offset at the IP given the position downstream as discussed in section 1.4.2.

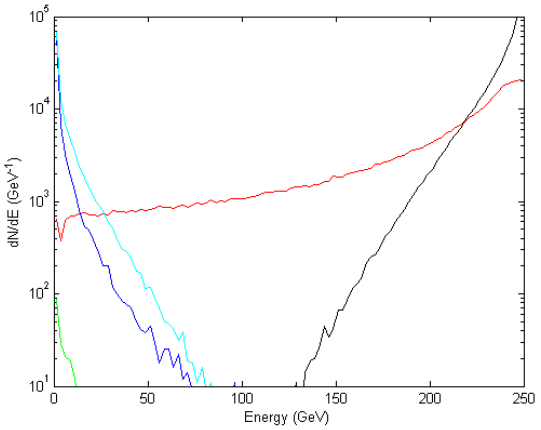
1.3.1 GUINEA PIG simulation of the beam-beam interaction

GUINEA PIG [27] simulates the beam-beam interaction of e^+ and e^- bunches with a given set of input parameters. This simulation tool includes the pinch effect, beam-beam kick, beamstrahlung, pair creation, bremsstrahlung, minijets and hadronic backgrounds [24]. The pairs are tracked through the fields of the beams.

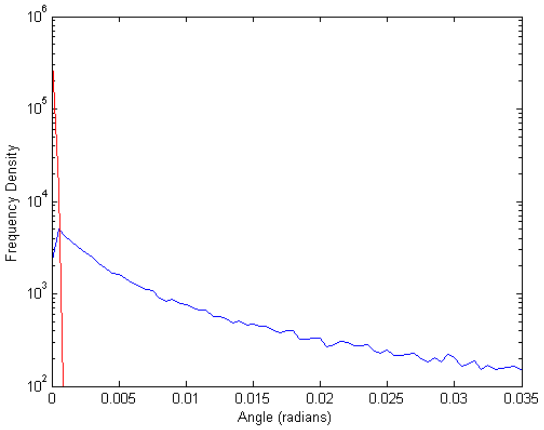
The output includes luminosity information, the disrupted outgoing beams and backgrounds. The output for the backgrounds is divided into separate files: pairs, bremsstrahlung leptons, hadrons, minijets and photons. The energy distribution for these outputs is shown in figure 1.3(a) for the ILC with 500 GeV centre of mass energy. Here, 0.005% of the disrupted beam (black) is shown, where energy loss has been due to beamstrahlung. The backgrounds are for a full bunch crossing of 2×10^{10} electrons and 2×10^{10} positrons. Bremsstrahlung leptons (red) follow the exiting beam. The highest backgrounds are beamstrahlung and bremsstrahlung photons (light blue) and electron and positron pairs (dark blue). Hadron and minijet backgrounds (green) are low.

Figure 1.3(b) shows the angle distribution of the pairs and photons with respect to the outgoing angle of the beam. The photons are in a narrow cone that exits with the beam whereas the pairs have transverse momentum. The pairs from the beam-beam interaction are therefore a concern in terms of producing secondary backgrounds by interacting with materials in the interaction region.

There are some limitations to GUINEA PIG. Approximations are used to physical processes with many second order non-linear processes not included [25]. Polarisation of the beams is not considered. Work done with a similar beam-beam interaction simulation tool, CAIN [31], has indicated that including polarisation would reduce the pair backgrounds by 10-20% [25]. The reduction is seen as fewer low energy and low transverse momentum pairs.



(a) Number versus Energy for GUINEA PIG simulation outputs of a simulation of the ILC with 500 GeV centre of mass energy. Black: 0.005% of the spent beam. Red: Bremsstrahlung leptons. Light Blue/Cyan: Photons. Blue: Pairs. Green: Hadrons and minijets.



(b) The distribution of angle with respect to the outgoing beam of pairs (blue) and photons (red).

Figure 1.3: The output of a GUINEA PIG simulation of the beam-beam interaction for the ILC with 500 GeV centre of mass energy.

1.4 Feedback in the ILC Beam Delivery System

The beams at the ILC can be as small as 2.5 nm in σ_y (see table 1.3) so to achieve design luminosity, the beams must be stable in y at the IP at the sub-nanometre level. As shown in figure 1.4, the luminosity loss with a 0.5 σ_y offset is 10% according to beam-beam simulations with GUINEA PIG [27]. Keeping the beam stable within 0.1 σ_y would preserve most of the luminosity. The angle offset of the colliding beams also affects luminosity as shown in figure 1.5 which shows data from GUINEA PIG beam-beam simulations. Angle stability is therefore also required with the target stability being 0.1 σ'_y [32].

These stability goals are possible with multiple feedbacks in the beam delivery system (BDS) as described in 1.4.2.

1.4.1 Ground Motion and Cultural Noise Issues for Stabilisation

Stability must be maintained in the presence of component jitter, particularly in the BDS region where the optics are strong and magnet jitter has a large effect on the beam. Beamline components jitter due to ground motion (with wavelengths that are short compared to the distances between components) and noise from hardware both in and near the tunnel. This noise can be amplified by supports and common girders. Ground motion studies have been performed at various sites including the Stanford Linear Accelerator Center (SLAC) [34] to understand the extent of the problem for linear colliders.

Studies of the combined cultural noise and ground motion at SLAC show that natural ground motion and motion from the facilities tends to decrease in amplitude as frequency

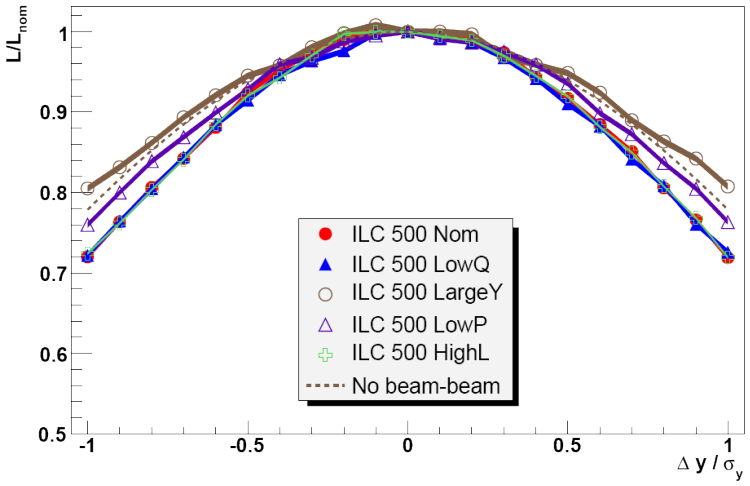


Figure 1.4: The luminosity normalised to its maximum vs vertical position offset as a fraction of the RMS beam size in y [33]. The five parameter sets for the 500 GeV centre of mass ILC are shown (as described in table 1.2) along with the calculation for luminosity ignoring the beam-beam effect.

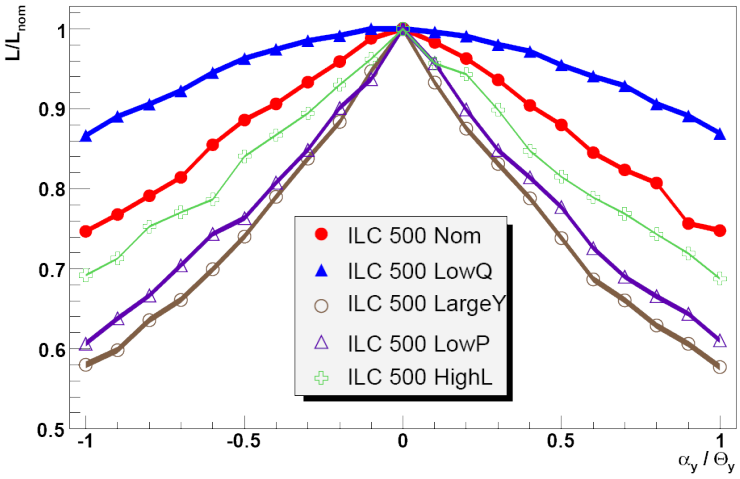


Figure 1.5: The luminosity normalised to its maximum vs vertical angle offset as a fraction of the RMS beam divergence in y [33]. The five parameter sets for the 500 GeV centre of mass ILC are shown (schemes 3-7 as described in table 1.2).

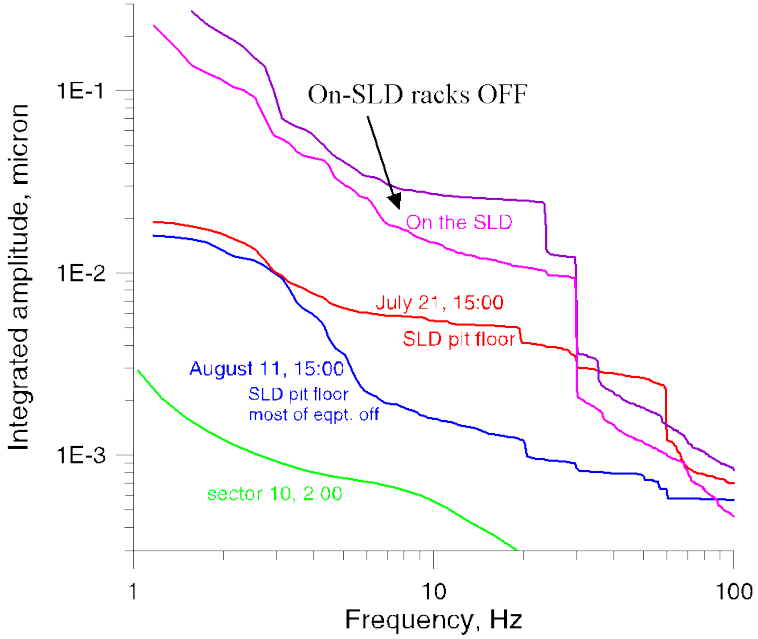


Figure 1.6: The integrated amplitude of the ground motion versus frequency is shown for various sites at SLAC [34]. The green "sector 10" curve is from data recorded at a very quiet location and so is more representative of the natural ground motion. The other curves are from data recorded on the SLAC Large Detector (SLD) with the electronics on (purple) and off (pink) and on the SLD pit floor with equipment on (red) and off (blue).

increases, as shown in figure 1.6. Most of the noise is local; the location with the least human activity (sector 10 of the SLAC linac, shown in green) has motion two orders of magnitude less than at the busiest location (the SLD detector, shown in purple), so careful design of the detector and facilities at the ILC should reduce vibrations. Further studies looking at the correlation between two points 100 m apart indicate that above 1 Hz, the wavelength of the vibrations is short enough that the effect on the beamline components is noise-like, figure 1.7. Below 1 Hz, the wavelength tends to be long so the correlation is very strong.

Being a dynamic effect, this component jitter requires a dynamic correction that steers the beam orbit within the timescale of the effect. Figure 1.6 indicates that the timescale of the nanometre-level displacement from cultural noise can be faster than the ILC (pulse) repetition rate of 5 Hz but much slower than the bunch frequency, nominally 3.25 MHz. The orbit of one bunch is therefore correlated with the next. However, successive pulse trains will be slightly uncorrelated due to this noise. A bunch-to-bunch dynamic correction based on feedback is therefore possible to maintain stability during the pulse train in the presence of noise from hardware and a 5 Hz feedback will be able to correct for the slow ground motion.

Figure 1.8 shows the luminosity (relative to the maximum) over time from simulations of the TESLA machine in the presence of ground motion and cultural noise. Luminosity is quickly lost without any feedback correction. The bunch-to-bunch correction (labeled IP FFBK) does not maintain the luminosity for long as the noise that is introduced between pulses alters the beam orbit in the BDS. Together the bunch-to-bunch feedback and a slow orbit correction can maintain stability and hence luminosity for a day before dispersion from

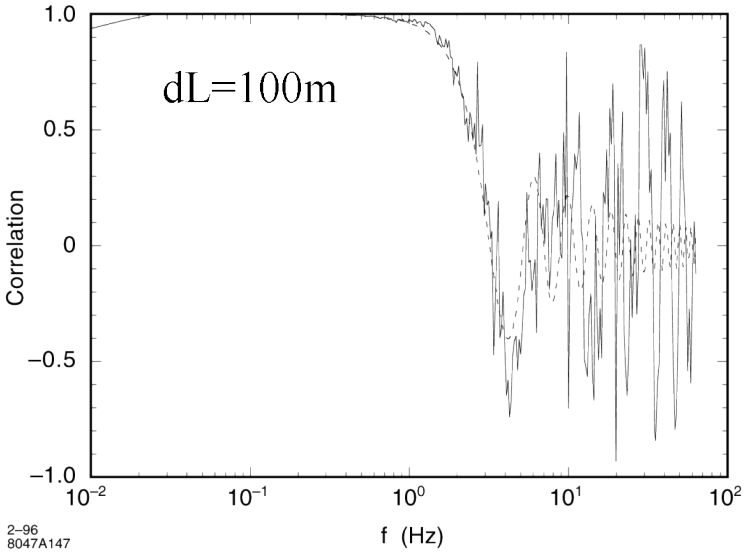


Figure 1.7: The correlation in ground movement at two points 100 m apart vs frequency [34]. The study was done in the Stanford Linear Collider tunnel.

the corrector kicks causes it to drop [15].

1.4.2 Intra-train Feedbacks at the ILC

The IP offset-correction feedback and IP angle-correction feedback are beam-based intra-(bunch)train feedbacks. They use a beam position monitor (BPM) to measure the position offset of the beam and deliver a kick to later bunches.

The hardware for IP offset-correction feedback consists of a BPM near the IP that measures the position of the outgoing bunches and a stripline kicker situated in the Final Focus Section that steers incoming bunches. This is shown schematically in figure 1.9 with an outgoing beam measured by a BPM, the signal processed and sent to a kicker on the incoming beam. The feedback BPM needs to be close to the IP to reduce latency, that is to provide fast corrections before too many bunches are lost. Having the BPM before any optics also helps to keep the correction simple as the position at the BPM is directly related to the position at the IP. Simulations of the beam-beam interaction with GUINEA-PIG have shown that an offset at the nanometre level at the IP produces a beam-beam kick that changes the angle of the exiting beam by tens of micro-radians [11]. With a BPM approximately three metres downstream, this nanometre offset is an offset of tens of microns in the BPM. Therefore, sub-nanometre stability at the IP (target stability is the 0.1 σ level) can be achieved with micron-level resolution in a BPM. The beams need to be within a certain range of each other for the fast position feedback to be effective. Simulations in GUINEA-PIG for each of the seven parameter sets at the 500 GeV ILC (see table 1.2) produced the amount of beam-beam kick expected for offsets of the beams in y as shown in figure 1.10. The feedbacks work most efficiently where angle kick increases with offset which is up to a 30 nm offset for the Low-Q set (shown in cyan) and up to a 170 nm offset in the Large Y set (shown in magenta) [32].

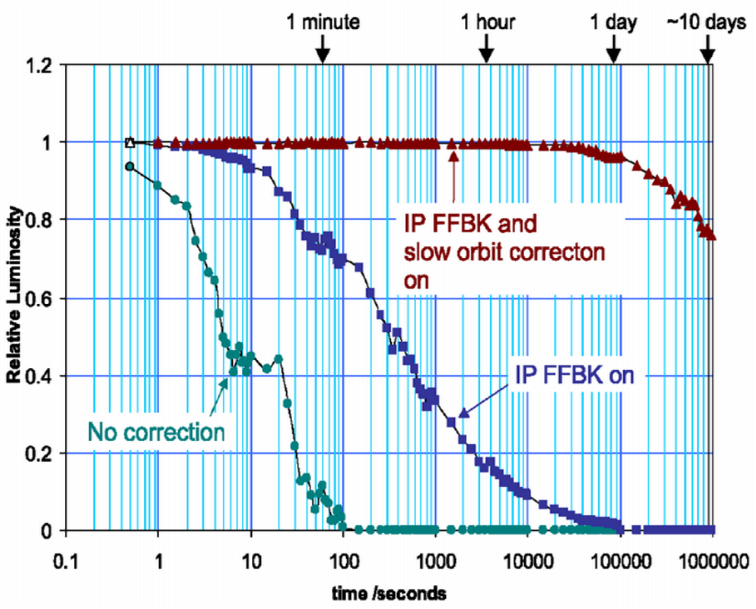


Figure 1.8: The luminosity vs time in the presence of ground motion [15]. Three cases are shown: without correction, with fast feedback correction of IP position and angle offset, and both fast feedback and slow feedback.

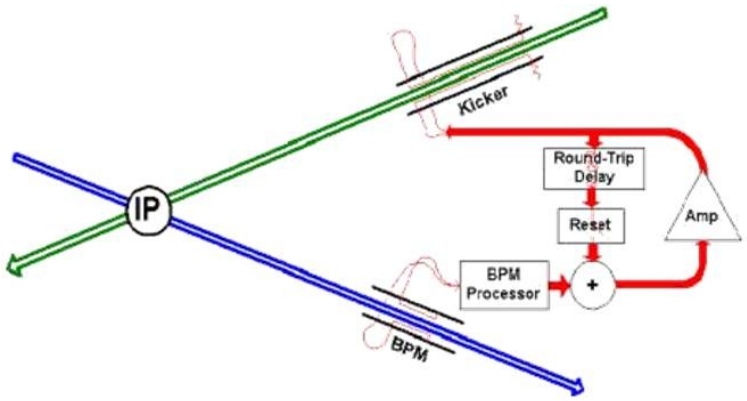


Figure 1.9: Block diagram of IP position feedback with the BPM on the extraction line and the kicker on the incoming beamline [35].

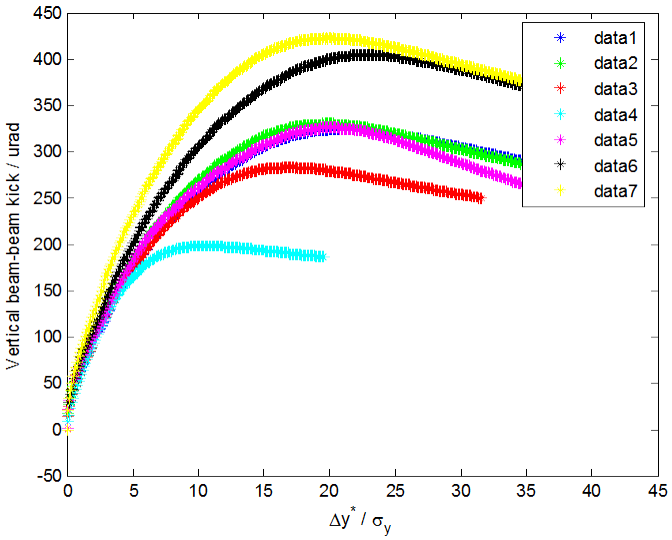


Figure 1.10: The angle that the beam-beam interaction gives to the beams versus the normalised vertical position offset [32]. The seven parameter sets as described in table 1.2 are shown. 1. TESLA (blue), 2. USSC (green), 3. Nominal (red), 4. Low Q (cyan), 5. Large Y (magenta), 6. Low P (black) and 7. High Luminosity (yellow).

The IP angle-correction feedback uses a stripline kicker at the same phase as the IP so that changes in angle given at the kicker relate to those given at the IP. The BPM needs to be downstream of the kicker and at a phase 90 degrees out of phase with the kicker and the IP. The angle offset will appear as a position offset in the BPM at that phase advance, so by zeroing the position in the BPM the angle at the IP is zeroed. This system will be placed at the entrance to the Final Focus System 1800 m upstream of the IP [32]. This is to take advantage of the large beta functions and hence the large position offset in the BPM, so that it is only required to have micron-level resolution for 0.1σ stability.

The capture range in which the IP offset-correction feedback works defines the performance requirements of the slow 5 Hz feedbacks. The 5 Hz feedbacks need to be able to recover the orbit to within this range. Once the slow feedbacks have converged within the range required by the fast feedbacks, the fast feedbacks will work.

Simulations have shown the effectiveness of the IP offset and angle corrections at recovering luminosity [36]. PLACET [37] was used to simulate beam dynamics with wakefields in the ILC linac in the presence of ground motion, injection jitter and alignment errors of the accelerating cavities, quadrupoles and BPMs up to 300 μm. Then the beam dynamics through the BDS was simulated, also with PLACET, with optics as for the ILC at a 14 mrad crossing angle. Finally the beam-beam interaction at the IP was simulated with GUINEA-PIG. The feedbacks were written in Matlab and Simulink [38].

Figure 1.11 shows how, bunch by bunch, the beam is steered until luminosity is at its maximum. The initial offsets of the beam in position and angle are removed by bunch 100. After the beam has been steered to zero position and angle offset, there are scans in position and angle (around bunch 160 and 180 respectively) in case any more luminosity can be recovered. Previous simulations [32] have shown that some luminosity is recovered this way

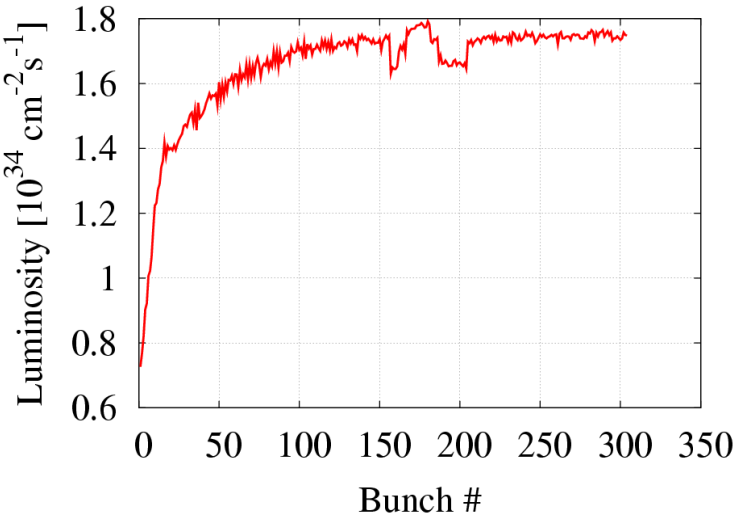


Figure 1.11: The luminosity versus bunch number with intra-train feedback in the presence of ground motion [36].

because wakefield effects in the TESLA accelerating cavities cause a y-z correlation within each bunch (the "banana effect"). With the beams no longer being Gaussian, the offset and angle at the IP for maximum luminosity is non-zero and scanning in the two dimensions of position and angle can optimise luminosity with the aid of a luminosity monitor. However, in the ILC linac simulation, wakefield effects appear not to be as strong [36].

It is not possible to achieve the luminosity calculated with perfect head-on collisions of Gaussian beams; the feedbacks require time to work and any bunch-to-bunch jitter will be magnified by the feedback.

The recovery of luminosity using these two fast feedbacks is less effective with greater jitter on the main linac quadrupoles. Simulations were done in PLACET for the beam dynamics in the TESLA linac (with wakefields) and the TESLA IR, and the beam-beam interaction was simulated with GUINEA-PIG [29]. Figure 1.12 shows that the luminosity decreases with increased jitter on the main linac quadrupoles (shown in red). Some luminosity (around 5%) is recovered with an offset-correction feedback (shown in green) and some more is gained through the angle-correction (blue). Scans in y (magenta) and y' (cyan) recover more luminosity but 13% is still lost at 100 nm of quadrupole jitter. The remainder can be recovered with intra-pulse feedback before the BDS (shown in black). This correction at the end of the linac and before the BDS is in both y and y' to the 0.1 σ level and is referred to as the "train straightener" [11].

1.5 Beam Position Monitors

Beam position monitors (BPMs) are a vital part of the feedback systems as well as being essential for machine diagnostics. There are many different BPMs, the most common being button, stripline and cavity.

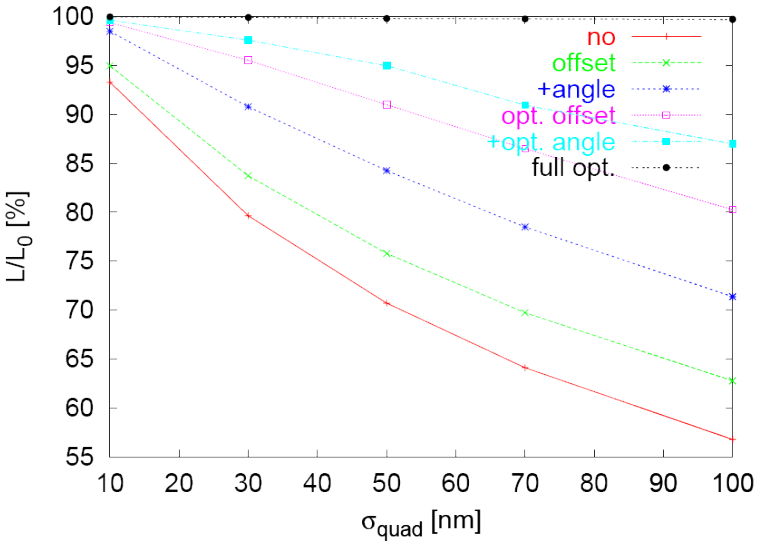


Figure 1.12: The luminosity normalised to the maximum luminosity versus RMS jitter on the main linac quadrupoles [29]. The luminosity can be recovered (from red) using feedbacks in IP y offset (green), feedbacks in IP y' offset (blue), luminosity optimisation with y (magenta), luminosity optimisation with y' (cyan) and a train straightener at the end of the linac (black).

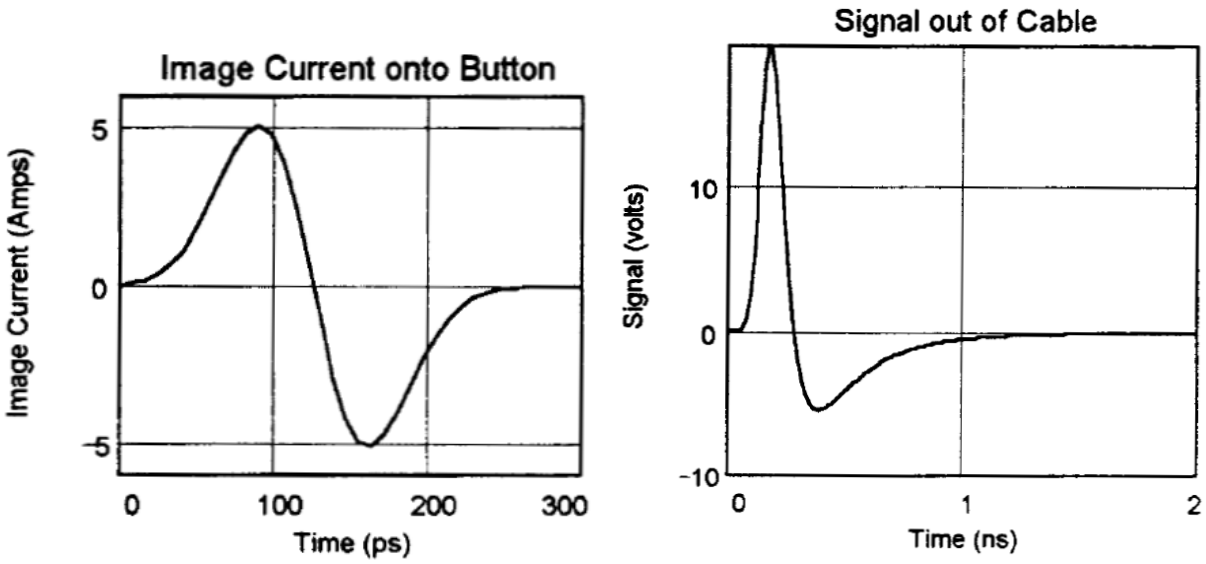
1.5.1 Button BPMs

Button BPMs are essentially electrodes that break the continuity of the beampipe wall. As the name implies, this BPM looks like a button.

As a charged beam travels down the beampipe, associated electric and magnetic fields travel with it. The electric field is Lorentz contracted at relativistic velocities such that the electric and magnetic fields are transverse to the direction of motion [39]. This "pancake" shaped electric field intersects with the beampipe with the beam causing an induced current to travel on the wall of the beampipe. This induced current moves at the same speed as the beam. The integral of the induced current around the circumference of the beampipe is equal to the beam current but it is not distributed evenly if the particle is off-centre. The induced current can be used to monitor the position of the beam as the closer to the beampipe the beam is, the more dense the electric field and the greater the current density at that point.

The beam's induced current, travelling along the wall of the beampipe, meets a discontinuity at the button BPM and jumps the gap onto the button. The button is not grounded so the net charge on the button must be zero. A current is set up on the button BPM with one polarity when the charge hops onto the BPM and the reverse polarity when it hops off and onto the beampipe wall (as shown in figure 1.13(a) for a bunch with an approximately Gaussian longitudinal distribution) [40]. As the button BPM is very small, this bipolar current is very fast.

The signal voltage on the button BPM is affected by the capacitance of the button BPM and the signal from the BPM pickoff, usually transported far from the beampipe to the processing electrons via a cable with losses at high frequencies, does not appear as a perfect bipolar voltage signal [40]. Instead, it appears as a sharp peak followed by a small and broad



(a) The current on the button BPM with time.

(b) The signal from the button BPM after it is passed through a long cable.

Figure 1.13: The button BPM response to a passing beam of charged particles [40].

peak with the opposite polarity as shown in figure 1.13(b).

As described above, the image charge intercepted depends on the position of the beam. Therefore, the voltage signal from the button BPM can be used to monitor the beam position. The change in voltage signal at a button BPM due to a change in position is a small amount on top of a large voltage signal. Therefore the usual method of extracting the change in signal is to use two electrodes diametrically opposite each other. The difference of the signals from the two electrodes is dependent on the magnitude of the beam charge and the position offset. To remove the dependence on the beam charge, the sum of the signals (which is charge dependent only) can be used to normalise the difference signal [41].

The difference (or normalised difference) needs to be processed to near DC frequencies to be used as an indicator of position. Matlab was used to simulate a perfect processing scheme (without noise or losses) in order to find the intrinsic resolution[2] of a button BPM. It was found to be $\sim 0.5\mu$m [40] for this perfect case. Practically, this is not attainable not only due to losses and noise in the processor electronics but also due to imperfections in the construction of the button BPM and impedance mismatches.

The advantage of a button BPM is its compact size. As space is at a premium at the ILC, the button BPM is considered for the feedback BPM should a stripline BPM not fit.

1.5.2 Stripline BPMs

A stripline BPM interrupts the beampipe and intercepts the induced current similar to the button BPM. As the beam passes the stripline, the induced current moves from the beampipe to the stripline. Once the beam has passed the stripline, the induced current moves back to

[2]The resolution is the smallest deflection of the beam a BPM can measure.

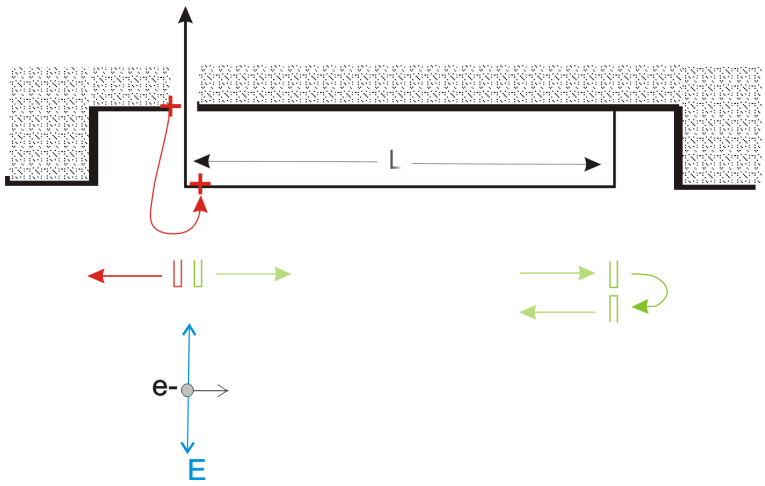


Figure 1.14: The production of a signal from an electron on a stripline with the downstream end shorted.

the beampipe.

From one stripline BPM to the next, the strips can differ in length, width and distance of the stripline from the beampipe wall. The length of the stripline affects the frequency response of the BPM as discussed in section 1.5.2. The width is often large as it is preferable to cover as much of the beampipe inner surface as possible to maximise the amount of induced charge that is on the stripline. To keep the impedance of the stripline high (standard is 50 Ω), the height of the stripline is raised from the ground plane [39]. High impedance results in good sensitivity as induced voltages are high.

Stripline designs also differ at their ends in terms of the upstream and downstream termination. The end of a stripline can be, as any transmission line, shorted, left open or terminated through a resistance (across which the voltage can be measured to extract a signal). The method of production of the stripline signal varies slightly depending on the termination [42].

Stripline BPMs have a better intrinsic resolution (∼0.05 nm) than button BPMs [35]. They are not as compact length-wise (being obviously a longer device) but are just as compact in the transverse direction making it the most likely candidate for the IP feedback BPM.

Stripline signal production

Figure 1.14 shows an electron with its "pancake" electric field (blue) approaching the upstream end of a stripline with a shorted downstream end. The induced charge (positive in charge and, when integrated over the circumference of the beampipe, equal in magnitude to the electron) follows the electron on the wall of the beampipe. The upstream end of the stripline as shown is a gap in the beampipe. Part of the induced charge (since the stripline only covers part of the beampipe) must cross the gap (as a displacement current) and continue on the stripline. The jump from wall to stripline induces a voltage of negative polarity in the stripline. The magnitude is related to the amount of induced charge intercepted by

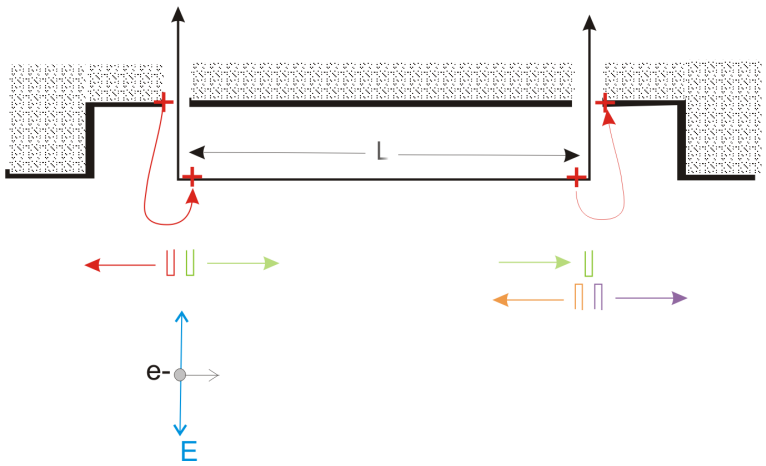


Figure 1.15: The production of a signal from an electron on a stripline with the downstream end terminated through matched impedance with the stripline.

the stripline. The voltage pulse splits into two, one travelling upstream (red) and the other downstream (green). Here the upstream end of the stripline is passed outside the beampipe to be terminated with an impedance matching that of the stripline (preventing reflections). The downstream travelling signal is reflected when it reaches the shorted downstream end and its polarity is reversed (the reflection coefficient of a shorted transmission line is -1). The reversed signal travels upstream and arrives at the upstream end at a time approximately $2L/c$ later than the initial signal (red). Thus the output of the stripline is a negative voltage pulse followed by a positive one of the same magnitude $2L/c$ later.

Figure 1.15 shows an electron approaching the upstream end of a stripline with the downstream end terminated through an impedance matched with that of the stripline. The scenario is the same at the upstream end of the stripline. However, the downstream travelling signal is not reflected. With relativistic beams, the velocity of the beam particle and the phase velocity of the stripline match. The electron will arrive at the downstream end of the stripline at the same time as the downstream travelling signal arrives. The induced charge crosses from the stripline to the beampipe wall, the reverse of the action at the upstream end. This induces a voltage signal with the reverse polarity. The voltage signal splits with half travelling upstream (orange) and a half travelling downstream (purple). This downstream travelling signal is equal in magnitude but opposite in polarity to the downstream travelling signal from the upstream end (green) and so the two signals cancel resulting in no signal at the downstream pick-off. The upstream travelling pulse (orange) arrives at the upstream end at a time approximately $2L/c$ later than the initial signal (red). Thus the output of the stripline is a negative voltage pulse followed by a positive one of the same magnitude $2L/c$ later, identical to the previous description.

Figure 1.16 shows an electron approaching the upstream end of a stripline with the downstream end open. The scenario is, again, the same at the upstream end of the stripline. The downstream travelling signal is reflected when it reaches the downstream end but its polarity is not reversed (the reflection coefficient of an open transmission line is +1). The induced charge crosses from the stripline to the beampipe wall inducing a voltage signal with the reverse polarity. The voltage signal splits with half travelling upstream (orange) and a half

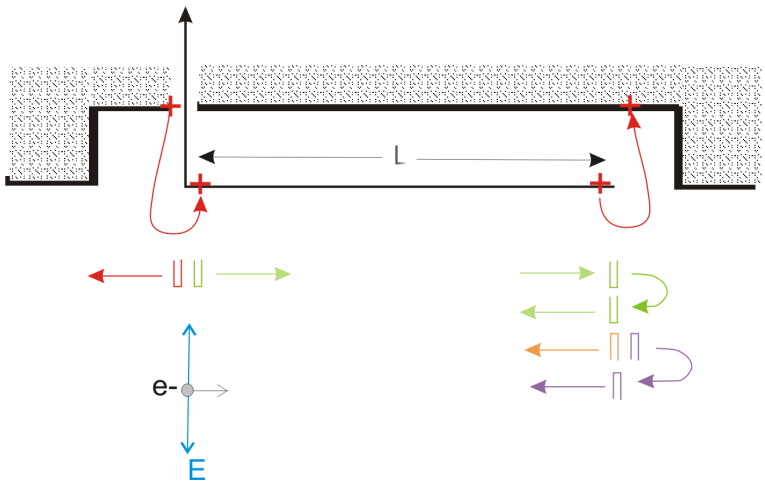


Figure 1.16: The production of a signal from an electron on a stripline with the downstream end open.

travelling downstream (purple). This upstream travelling signal (orange) is equal in magnitude but opposite in polarity to the downstream travelling signal from the upstream end (green) and so the two signals cancel. The downstream travelling signal from the downstream end (purple) is reflected and arrives at the upstream end at a time approximately $2L/c$ later than the initial signal (red). Thus the output of the stripline is a negative voltage pulse followed by a positive one of the same magnitude $2L/c$ later, identical to the two previous descriptions.

These striplines result in identical signals from a passing beam but would treat other sources of signal differently. A signal from a particle hit, for example, would not result in identical signals for these three types. Here, there would not be an induced charge jumping from beampipe to stripline back to beampipe. Instead there is one voltage pulse that is split, half upstream travelling and half downstream travelling, and the downstream travelling pulse is either reflected or transmitted depending on the end load to the transmission line. Figure 1.17 shows a voltage signal being created by an electron hit (red, the upstream-going pulse and green, the downstream-going pulse) on each stripline type as described. The differences come from the different ways the downstream end is terminated. With a shorted end, the signal from the electron hit is reflected and inverted. With an open end, the signal from the electron hit is reflected but not inverted. With the end terminated through a matched impedance, the signal is not reflected at all and can be seen as a signal on the downstream pick-off.

The striplines with shorted and open ends could be reversed with the downstream end being used as the pickup. The signal from the shorted case with the downstream end as the pick-off has a positive voltage pulse followed by a negative voltage pulse for a negatively charged beam. The stripline where the downstream end is terminated through matching impedance does not have any signal at the downstream end which makes it ideal for use in a circular machine with two beams in opposite direction as both pick-offs can be used, one receiving the signal from the beam travelling in one direction and the other receiving the signal from the beam travelling in the other direction.

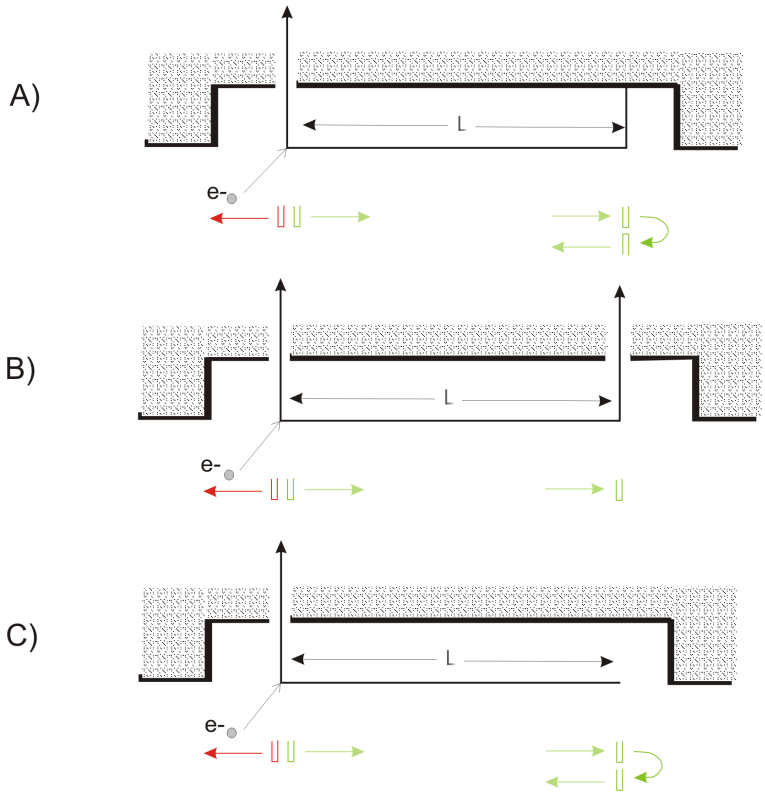


Figure 1.17: The signal from an electron hitting the upstream end of a stripline with A) the downstream end shorted, B) the downstream end terminated and C) the downstream end open.

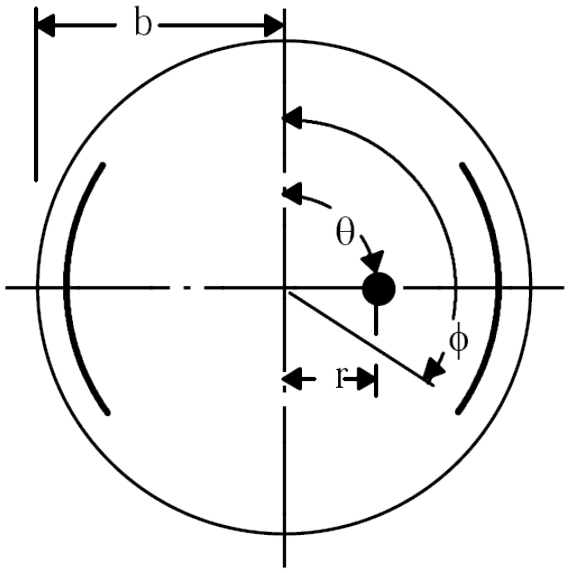


Figure 1.18: Cross-section of a beampipe (radius b) with striplines mounted on the side (as marked by dark lines) and a beam a distance r from the centre of the beampipe [39]. The striplines subtend an angle $\alpha = 2(\phi - \theta)$.

The response of the stripline to offset beams

The beam current (I_{beam}) can be approximated as a Dirac impulse in longitudinal distance z for short enough bunches of bunch charge q:

$$I_{\text{beam}} = qc\delta(z) \tag{1.8}$$

The current in the stripline has the magnitude of the fraction of induced current intercepted by the stripline subtending an angle $\alpha = 2(\phi - \theta)$ with the angles defined in figure 1.18. For a beam that goes down the centre of the beampipe this is simply $\frac{I_{\text{beam}}\alpha}{2\pi}$ but for an offset beam as shown in figure 1.18, the stripline current is given by [43]:

$$I_{\text{stripline}}(r) = \frac{I_{\text{beam}}}{2\pi}(b^2 - r^2)\int_{-\frac{\alpha}{2}}^{\frac{\alpha}{2}} \frac{d(\frac{\alpha}{2})}{b^2 + r^2 - 2br\cos(\frac{\alpha}{2})} \tag{1.9}$$

If r << b, this can be approximated:

$$\begin{aligned} I_{\text{stripline}}(r) &\approx \frac{I_{\text{beam}}}{2\pi}\int_{-\frac{\alpha}{2}}^{\frac{\alpha}{2}} 1 + 2\frac{r}{b}\cos\left(\frac{\alpha}{2}\right) d\left(\frac{\alpha}{2}\right) \\ &= \frac{I_{\text{beam}}}{2\pi}\left(\alpha + \frac{4r}{b}\sin\left(\frac{\alpha}{2}\right)\right) \end{aligned} \tag{1.10}$$

The second term in equation 1.10 is the change in current due to an offset beam. By multiplying the current change with the characteristic impedance of the stripline (Z_0), the change in voltage from the pickoff can be expressed as in equation 1.11. Taking the case of the stripline shorted at the downstream end, I_{beam} has been expanded as two Dirac impulses

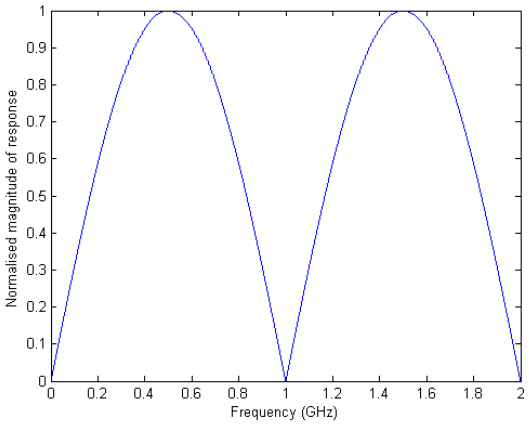


Figure 1.19: The frequency response of a 15 cm stripline normalised to its maximum value (see equation 1.12).

for the signal at the upstream end and the signal with the opposite polarity 2L/c later. The voltage signal is also divided by two as it splits into two equal pulses.

$$\Delta V(z,r) = \frac{Z_0 qcr}{\pi b} \sin\left(\frac{\alpha}{2}\right) \left(\delta(z) - \delta\left(z - 2L\right)\right) \tag{1.11}$$

The Fourier transformation of equation 1.11 is shown in equation 1.12 and figure 1.19. A stripline BPM is usually operated near the frequency that contains the most power (500 MHz is the best operating frequency of a 15 cm stripline as shown in figure 1.19).

$$\Delta V(k,r) = \frac{1}{2\pi} \frac{2Z_0 qcr}{\pi b} \sin\left(\frac{\alpha}{2}\right) \exp\left(i\frac{\pi}{2}\right) \exp(-ikL) \sin\left(kL\right) \tag{1.12}$$

1.5.3 Cavity BPMs

Cavity BPMs work on a different principle from stripline and button BPMs and are capable of much better position resolution [43].

When a bunch of charged particles passes through a RF cavity, EM fields are generated that set up standing waves. Since the charges are relativistic, the fields are transverse. The modes depend on the shape of the cavity as well as the beam charge, beam position offset, the bunch length, the bunch shape and the bunch spacing [41]. The modes that are set up in the resonant cavity are mainly TM010 (the monopole or fundamental mode) with some TM110 (the dipole mode). The monopole mode has an amplitude that is dependent on charge and needs to be suppressed in the processing electronics to extract the smaller dipole mode. The dipole mode has an amplitude that is dependent on charge and relative beam position from zero. The phase of the dipole mode relative to the monopole mode can measure the polarity of the position offset. The amplitudes and phases can be measured with antennae resonant at the appropriate frequencies to pick off the modes.

Cavity BPMs have recorded resolutions down to 20 nm [44] for single bunch extractions. For use with bunch trains, the excited signal of the cavity BPM needs to decay sufficiently in the time between bunches to allow the bunches to be resolved. Reentrant cavity BPMs are better suited to resolve individual bunches. The geometry of reentrant cavities is similar to a stripline BPM and the fields generated are below the resonant frequency of the cavity. The mode that is detected is the evanescent mode TE011 [41].

Cavity or reentrant cavity BPMs would not be appropriate as the ILC feedback BPM in terms of physical size; they are less compact than striplines or button BPMs.

1.6 Summary

The ILC is a proposed electron-positron collider with a centre of mass energy of 500 GeV with the possibility of an upgrade to 1 TeV. It will take the discoveries of the LHC further, making precise measurements of terascale physics.

The beam-beam interaction when the beams interact creates backgrounds through beamstrahlung and subsequent pair generation from the beamstrahlung photons. It also produces a beam-beam kick that is linearly dependent on the relative offset of the beams for small offsets (figure 1.10). This relation between offset and angle allows the use of a micron-resolution beam position monitor (BPM) a few metres away from the IP to infer the offset at the IP.

The flat beams of the ILC will be affected by ground motion and cultural noise at low frequencies as shown in figure 1.6 resulting in a loss of luminosity in a few seconds (figure 1.8). To restore luminosity, intra-train feedback is required.

The IP position feedback, illustrated in figure 1.9, uses a BPM to measure the position of an outgoing beam, related to its offset at the IP due to the beam-beam kick. The position is then used to kick the incoming beam, correcting the offset. Simulations have demonstrated that luminosity can be restored within a hundred bunches through this method (figure 1.11).

There are many BPM devices. Button BPMs are compact and well suited for the space-restricted ILC interaction region in that sense but micron-level resolution is technically hard to achieve. Stripline BPMs have better resolution and are still relatively compact. Cavity BPMs are capable of much better resolution than the feedback BPM requires and are larger so are not considered for this purpose.